ISSN 1674-1056
http://cpb.iphy.ac.cn
http://iopscience.iop.org/cpb
中国物理 B
Chinese Physics
中国物理 Chinese Physics B

Micromagnetic simulations of reversal magnetization in cerium-containing magnets

Lei Li(李磊), Shengzhi Dong(董生智), Hongsheng Chen(陈红升), Ruijiao Jiang(姜瑞姣), Dong Li(李栋), Rui Han(韩瑞), Dong Zhou(周栋), Minggang Zhu(朱明刚), Wei Li(李卫), Wei Sun(孙威)

Citation: Chin. Phys. B . 2019, 28(3): 037502. **doi:** 10.1088/1674-1056/28/3/037502
Journal homepage: http://cpb.iphy.ac.cn; http://iopscience.iop.org/cpb

What follows is a list of articles you may be interested in

Realization of artificial skyrmion in CoCrPt/NiFe bilayers

Yi Liu(刘益), Yong-Ming Luo(骆泳铭), Zheng-Hong Qian(钱正洪), Jian-Guo Zhu(朱建国)

Chin. Phys. B . 2018, 27(12): 127503. **doi:** 10.1088/1674-1056/27/12/127503

Dynamic nucleation of domain-chains in magnetic nanotracks

Xiangjun Jin(金香君), Yong Li(李勇), Fusheng Ma(马付胜)

Chin. Phys. B . 2018, 27(12): 127504. **doi:** 10.1088/1674-1056/27/12/127504

Interfacial effect on the reverse of magnetization and ultrafast demagnetization in Co/Ni bilayers with perpendicular magnetic anisotropy

Zi-Zhao Gong(弓子召), Wei Zhang(张伟), Wei He(何为), Xiang-Qun Zhang(张向群), Yong Liu(刘永), Zhao-Hua Cheng(成昭华)

Chin. Phys. B . 2018, 27(5): 057501. **doi:** 10.1088/1674-1056/27/5/057501

Effects of dipolar interactions on magnetic properties of Co nanowire arrays

Hong-Jian Li(李洪健), MingYue(岳明), Qiong Wu(吴琼), Yi Peng(彭懿), Yu-Qing Li(李玉卿), Wei-Qiang Liu(刘卫强), Dong-Tao Zhang(张东涛), Jiu-Xing Zhang(张久兴)

Chin. Phys. B . 2017, 26(11): 117503. **doi:** 10.1088/1674-1056/26/11/117503

Faster vortex core switching with lower current density using three-nanocontact spin-polarized currents in a confined structure

Hua-Nan Li(李化南), Zhong Hua(华中), Dong-Fei Li(李东飞)

Chin. Phys. B . 2017, 26(1): 017502. **doi:** 10.1088/1674-1056/26/1/017502

Micromagnetic simulations of reversal magnetization in cerium-containing magnets*

Lei Li(李磊)[1], Shengzhi Dong(董生智)[1,†], Hongsheng Chen(陈红升)[1], Ruijiao Jiang(姜瑞姣)[1], Dong Li(李栋)[1], Rui Han(韩瑞)[1], Dong Zhou(周栋)[1], Minggang Zhu(朱明刚)[1,2], Wei Li(李卫)[1,2], and Wei Sun(孙威)[2]

[1] *Division of Functional Materials Research, Central Iron and Steel Research Institute, Beijing* 100081, *China*
[2] *National Engineering Research Center for Magnetic Materials, Beijing* 102600, *China*

(Received 10 October 2018; revised manuscript received 9 January 2019; published online 22 February 2019)

Single-grain models with different cerium contents or structural parameters have been introduced to investigate the reversal magnetization behaviors in cerium-containing magnets. All the micromagnetic simulations are carried out via the object oriented micromagnetic framework (OOMMF). As for single $(Nd,Ce)_2Fe_{14}B$ type grain, the coercivity decreases monotonously with the increase of the cerium content. Four types of grain structure have been compared: single $(Nd,Ce)_2Fe_{14}B$ type, core ($(Nd,Ce)_2Fe_{14}B$)–shell ($Nd_2Fe_{14}B$) type with 2 nm thick shell, core ($Ce_2Fe_{14}B$)–shell ($Nd_2Fe_{14}B$) type, and core ($Nd_2Fe_{14}B$)–shell ($Ce_2Fe_{14}B$) type. It is found that core ($(Nd,Ce)_2Fe_{14}B$)–shell ($Nd_2Fe_{14}B$) type grain with 2 nm thick shell always presents the largest coercivity under the same total cerium content. Furthermore, the relationship between the coercivity and the shell thickness t in core ($(Nd,Ce)_2Fe_{14}B$)–shell ($Nd_2Fe_{14}B$) type grain has been studied. When the total cerium content is kept at 20.51 at.%, the analyzed results show that as t varies from 1 nm to 7 nm, the coercivity gradually ascends at the beginning, then quickly descends after reaching the maximum value when $t = 5$ nm. From the perspective of the positions of nucleation points, the reasons why t affects the coercivity are discussed in detail.

Keywords: micromagnetic simulation, cerium-containing magnets, core-shell structure, coercivity

PACS: 75.78.Cd, 75.50.Ww, 75.78.–n **DOI:** 10.1088/1674-1056/28/3/037502

1. Introduction

Among commercial magnets, Nd–Fe–B permanent magnets generally exhibit outstanding magnetic performance.[1] It is reported that Nd–Fe–B magnets have been widely used in many fields, such as electric vehicles, loudspeakers, hard disk drives, etc.[2–4] However, due to the massive consumption of neodymium, substantial cerium has been overstocked. In order to achieve a more balanced utilization of rare earths, many investigations have been carried out to use less Nd by adding Ce, which is cheaper and more abundant.[5–9]

Since the substitution of Ce for Nd in $Nd_2Fe_{14}B$ would result in smaller magnetocrystalline anisotropy, it is expected to find effective methods to enhance the coercivity of cerium-containing magnets. In early studies,[10–13] cerium-containing magnets prepared via a traditional powder metallurgy process exhibited poor magnetic properties. After a long period of exploration, strip casting (SC) + hydrogen decrepitation (HD) + jet milling (JM) process has been proven to assist in obtaining better magnetic properties in cerium-containing magnets.[14] In recent years, Li *et al.* invented the dual main phase alloy method and have conducted a lot of studies focusing on low-cost cerium-containing magnets.[15–19]

In addition to numerous technical innovations,[20,21] many materials calculations about cerium-containing magnets have been performed.[22,23] For example, Liu *et al.* studied the influences of microstructural and magnetic parameters of the grain boundary phase on the magnets by the finite element method.[22] However, there are few detailed reports about the internal grain structure of cerium-containing magnets. In this paper, via micromagnetic simulations, we explore the effects of cerium content, grain structure, and shell thickness on the coercivity of single-grain cerium-containing magnets. It is expected to deliver a preferable grain structure to offer effective assistance for practical experiments.

2. Simulation system and method

All the micromagnetic simulations are performed via the oriented object micromagnetic framework (OOMMF),[24] which works on the basis of the finite difference method. The Landau–Lifshitz–Gilbert (LLG) equation[25] is used for the magnetization reversal calculation. All the cerium-containing $Nd_2Fe_{14}B$ grains are modeled as cubes with the same side length of 39 nm. Four types of single-grain structures (Fig. 1), without grain boundary phases or neighbouring grains, are discussed in this paper.

For all grains, the intrinsic magnetic parameters at room temperature have been set as follows. For $Nd_2Fe_{14}B$, the anisotropy constant $K_1 = 4.5$ MJ/m, the saturation magnetization $\mu_0 M_s = 1.61$ T, and the exchange stiffness $A = 12.5$ pJ/m;[26] for $Ce_2Fe_{14}B$, $K_1 = 1.5$ MJ/m, $\mu_0 M_s = 1.17$ T,

*Project supported by the National Natural Science Foundation of China (Grant Nos. 51590882 and 51871063).
†Corresponding author. E-mail: dong_shengzhi@163.com
© 2019 Chinese Physical Society and IOP Publishing Ltd

and $A = 5$ pJ/m;[27] for $(Nd,Ce)_2Fe_{14}B$, K_1, $\mu_0 M_s$, and A are supposed to be in line with the atomic percentage ratio of Nd to Ce. In order to ensure the rationality for the solution of Brown's equation, the discretization cell size is set as 1 nm×1 nm×1 nm, which is smaller than the domain wall width l_w and the magnetostatic exchange length l_{ex}. Note that

$$l_w = \pi\sqrt{A/K_1},$$

$$l_{ex} = \sqrt{2A/(\mu_0 M_s^2)}.$$

For $Nd_2Fe_{14}B$, $l_w = 5.24$ nm and $l_{ex} = 3.48$ nm; for $Ce_2Fe_{14}B$, $l_w = 5.74$ nm and $l_{ex} = 3.03$ nm. The initial magnetization is oriented along the positive z-axis. During the reversal processes, the external field H_{ext} that is antiparallel with the initial magnetization is evenly applied from 0 (remanent state) to −10 T within 200 stages.

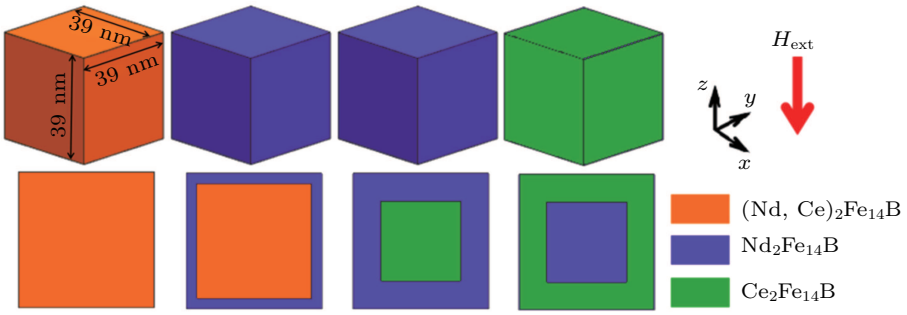


Fig. 1. Schematics for four types of grain structure: (a) single $(Nd,Ce)_2Fe_{14}B$ type, (b) core ($(Nd,Ce)_2Fe_{14}B$)–shell ($Nd_2Fe_{14}B$) type, (c) core ($Ce_2Fe_{14}B$)–shell ($Nd_2Fe_{14}B$) type, and (d) core ($Nd_2Fe_{14}B$)–shell ($Ce_2Fe_{14}B$) type.

3. Results and discussion

3.1. Effect of cerium content

Isolated grains of single $(Nd,Ce)_2Fe_{14}B$ type (Fig. 1(a)) have been studied to investigate the influence of cerium content (atomic percentage of cerium in total rare earth elements) on the coercivity. As seen in Fig. 2, the reversal processes of grains with seven cerium contents are calculated respectively. It is found that the coercivity gradually decreases as the cerium content increases.

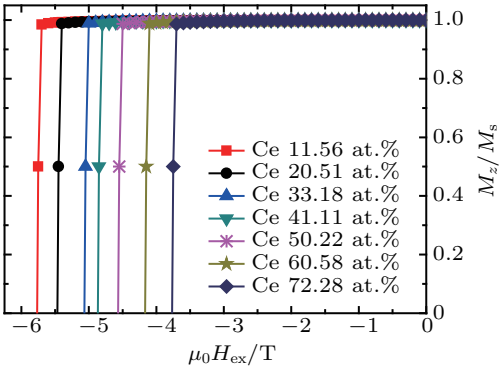


Fig. 2. The demagnetization curves for grains of single $(Nd,Ce)_2Fe_{14}B$ type with seven cerium contents.

Figure 3 illustrates that as cerium content increases, the coercivity exhibits the same tendency as the magnetocrystalline anisotropy field. It could be assumed that the sensitivity of the coercivity to the cerium content is mainly attributed to the magnetocrystalline anisotropy field. The larger cerium content leads to a smaller anisotropy field[15] of the isolated Nd–Fe–B grains, thus decreasing the nucleation field of the reverse domain, which results in the decrement of coercivity.

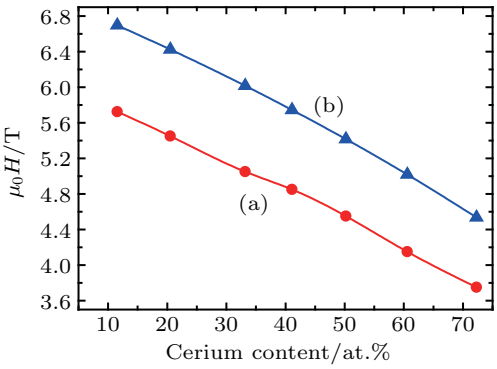


Fig. 3. The relevance of (a) the coercivity to the (b) magnetocrystalline anisotropy field under the same cerium content.

3.2. Effect of grain structure

To explore the effect of grain structure on the coercivity, four types of grain structure are compared: single $(Nd,Ce)_2Fe_{14}B$ type (Fig. 1(a)), core ($(Nd,Ce)_2Fe_{14}B$)–shell ($Nd_2Fe_{14}B$) type with 2 nm thick shell (Fig. 1(b)), core ($Ce_2Fe_{14}B$)–shell ($Nd_2Fe_{14}B$) type (Fig. 1(c)), and core ($Nd_2Fe_{14}B$)–shell ($Ce_2Fe_{14}B$) type (Fig. 1(d)). The total cerium content of isolated grains is set from about 10 at.% to about 60 at.%.

As shown in Fig. 4, for each type of grain, the coercivity remarkably deteriorates as the cerium content increases. It is obvious that with the same total cerium content, the coercivity of core ($(Nd,Ce)_2Fe_{14}B$)–shell ($Nd_2Fe_{14}B$) type with 2 nm thick shell is always the largest. Obviously, such core–shell structure is beneficial to enhancing the coercivity. To acquire the same coercivity, more cerium is permitted in core ($(Nd,Ce)_2Fe_{14}B$)–shell ($Nd_2Fe_{14}B$) type grain. For example, when the total cerium content of core ($(Nd,Ce)_2Fe_{14}B$)–shell

($Nd_2Fe_{14}B$) type grain is 60.58 at.%, the calculated coercivity is able to rival the one of single $(Nd,Ce)_2Fe_{14}B$ type grain with 50.22 at.% cerium and the one of core ($Ce_2Fe_{14}B$)–shell ($Nd_2Fe_{14}B$) type grain with 20.51 at.% cerium. In actual experiments, the grain boundary diffusion technique or dual alloy method is promising to achieve such core ($(Nd,Ce)_2Fe_{14}B$)–shell ($Nd_2Fe_{14}B$) type grain structure, and it is of great benefit to making effective use of Ce to obtain high coercivity and reducing the production cost.

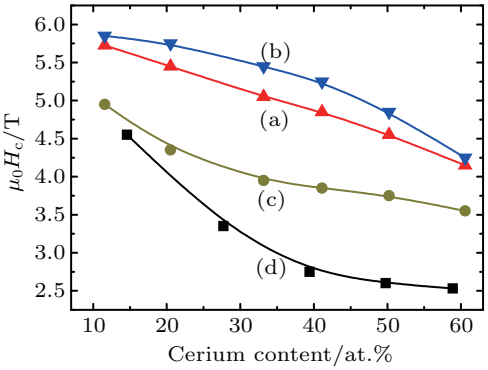


Fig. 4. Coercivity $\mu_0 H_c$ comparisons among four types of grains: (a) single $(Nd,Ce)_2Fe_{14}B$ type, (b) core ($(Nd,Ce)_2Fe_{14}B$)–shell ($Nd_2Fe_{14}B$) type with 2 nm thick shell, (c) core ($Ce_2Fe_{14}B$)–shell ($Nd_2Fe_{14}B$) type, and (d) core ($Nd_2Fe_{14}B$)–shell ($Ce_2Fe_{14}B$) type.

3.3. Effect of shell thickness

The core ($(Nd,Ce)_2Fe_{14}B$)–shell ($Nd_2Fe_{14}B$) type model has been introduced to discuss the dependence of coercivity on the $Nd_2Fe_{14}B$ shell thickness t while the grain size and total cerium content remain unchanged. The total cerium content of isolated grain is kept at 20.51 at.%. Due to the constant grain size and total cerium content, as the $Nd_2Fe_{14}B$ shell becomes thicker, the neodymium content in the core becomes smaller and the cerium content in the core becomes larger. The intrinsic magnetic properties and the volume fraction of the core are listed in Table 1. As t increases from 0, the grain structure is changed from single $(Nd,Ce)_2Fe_{14}B$ type (Fig. 1(a)) to core ($(Nd,Ce)_2Fe_{14}B$)–shell ($Nd_2Fe_{14}B$) type (Fig. 1(b)). When t reaches 8 nm, the chemical composition of the core is $Ce_2Fe_{14}B$, and the grain structure is core ($Ce_2Fe_{14}B$)–shell ($Nd_2Fe_{14}B$) type (Fig. 1(c)).

Table 1. The intrinsic magnetic parameters and the volume fractions of the core with different t values. Note that H_A is the magnetocrystalline anisotropy field.

t/nm	K_1/(MJ/m^3)	$\mu_0 M_s$/T	A/(pJ/m)	H_A/T	Volume fraction/%
1	3.78	1.50	10.70	6.316	85.39
2	3.65	1.48	10.37	6.176	72.28
3	3.48	1.46	9.96	5.995	60.58
4	3.28	1.43	9.44	5.756	50.22
5	3.00	1.39	8.76	5.430	41.11
6	2.65	1.34	7.87	4.971	33.18
7	2.17	1.27	6.66	4.293	26.34
8	1.50	1.17	5.00	3.225	20.51

As seen in Fig. 5, as t increases, the coercivity ascends in the beginning. When $t = 5$ nm, the coercivity reaches the largest value of 5.975 T. Then the coercivity decreases rapidly while t ranges from 5 nm to 8 nm. In theoretical reports on the hard/soft exchange spring system,[28–32] it has been found that when the thickness of the hard layer is larger than its domain wall width, the reversal magnetization process is not sensitive to the specific value of the hard layer. As for our work in this paper, it is assumed that the optimum shell thickness, $t = 5$ nm, might also be related to the domain wall width. We will explore the detailed relationship in future research.

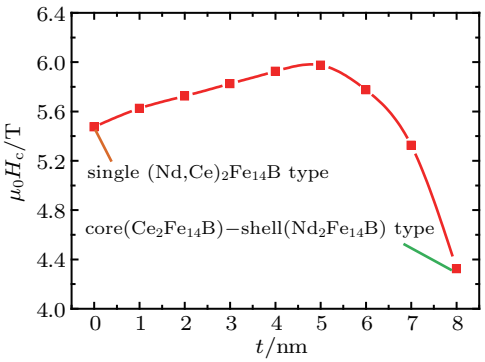


Fig. 5. The dependence of the coercivity $\mu_0 H_c$ on $Nd_2Fe_{14}B$ shell thickness t.

By calculating the dynamic evolution of magnetic moments over time, time resolved simulation is generally used to reveal the nucleation and the growth in the reversal process. Based on this method, the nucleation points are chosen to discuss the reasons why t affects the coercivity. The nucleation points for grains at different t are presented in view of x–z plane (Fig. 6). It is found that the nucleation points gradually propagate from the grain corner to the core center as t changes from 0 to 8 nm (Fig. 7). This phenomenon may be attributed to the relationship between the magnetocrystalline anisotropy field and demagnetization field.

Based on different positions of the nucleation points, the discussion comprises four parts: (I) grain corner, (II) grain edge, (III) core edge, and (IV) core centre.

(I) Grain corner: for $t = 0$–1 nm, the nucleation occurs at the corner of the grain. Figure 8 reveals the magnetization reversal process for $t = 1$ nm as an example. After nucleation, the reversal subsequently proceeds to the grain center. By comparing the chemistry of the nucleation points, it is obvious that pure $Nd_2Fe_{14}B$ for $t = 1$ nm possesses higher magnetocrystalline anisotropy field than $(Nd,Ce)_2Fe_{14}B$ (20.51 at.% cerium) for $t = 0$. Due to the positive relationship among the magnetocrystalline anisotropy field, nucleation field, and coercivity, the coercivity increases as t varies from 0 to 1 nm.

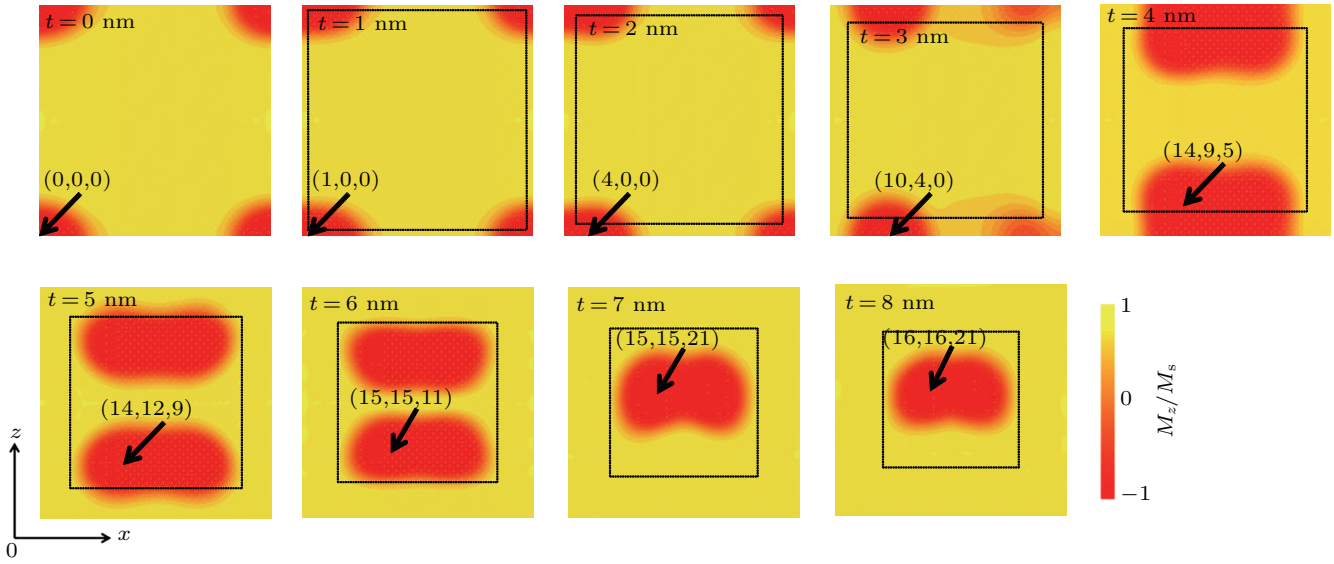


Fig. 6. Illustration of the nucleation points for $t = 0$–8 nm (view of x–z plane). The dotted lines represent the boundary between the shell and the core.

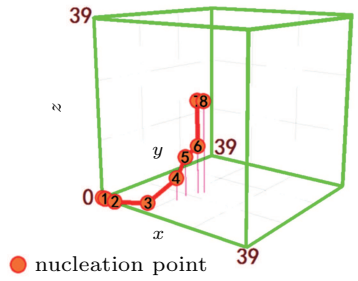


Fig. 7. Illustration of the nucleation point movement.

(II) Grain edge: for $t = 2$–3 nm, the nucleation occurs at the edge of the grain. The magnetization reversal process for $t = 3$ nm is demonstrated in Fig. 9. Different from $t = 1$ nm, $t = 2$ nm or $t = 3$ nm maintains a thicker shell of high anisotropy field, causing greater difficulty in rotating the moments of the shell. Thus, a larger external field is required to achieve the reversal magnetization processes.

(III) Core edge: for $t = 4$–5 nm, the nucleation occurs near the edge of the core. The reversal process for $t = 5$ nm is taken as an example in Fig. 8. Compared with $t = 3$ nm, the nucleation points of $t = 4$–5 nm are closer to the grain center and therefore present lower demagnetization fields. Moreover, for $t = 4$–5 nm, the boundary between the core and the shell strengthens the exchange coupling effect among the magnetic moments. The above two reasons are assumed to lead to the increase of coercivity.

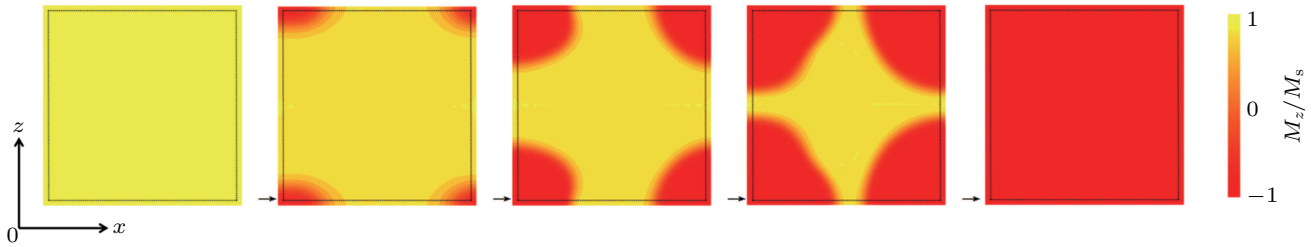


Fig. 8. The reversal process for $t = 1$ nm (view of x–z plane at $y = 0$) under the external field of 5.625 T (equal to the coercivity).

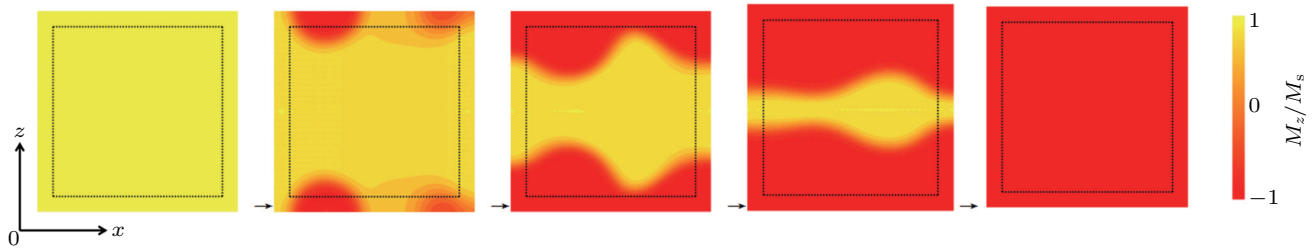


Fig. 9. The reversal process for $t = 3$ nm (view of x–z plane at $y = 4$ nm) under the external field of 5.825 T (equal to the coercivity).

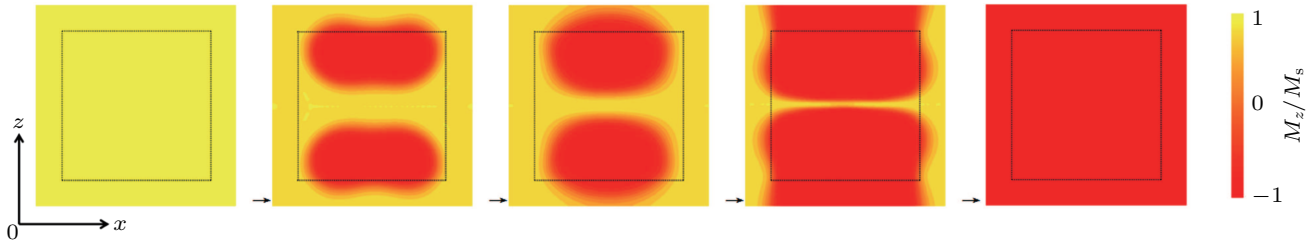


Fig. 10. The reversal process for $t = 5$ nm (view of x–z plane at $y = 12$ nm) under the external field of 5.975 T (equal to the coercivity).

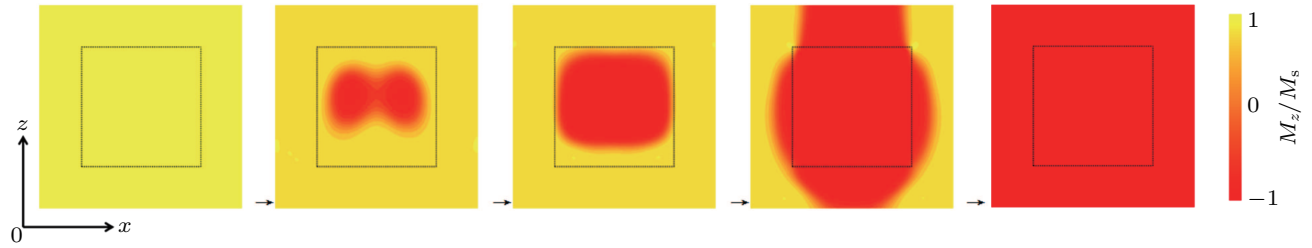


Fig. 11. The reversal process for $t = 8$ nm (view of x–z plane at $y = 16$ nm) under the external field of 4.375 T (equal to the coercivity).

(IV) Core center: for $t = 6$–8 nm, the nucleation occurs close to the center of the core. Figure 11 indicates the reversal process for $t = 8$ nm. It is seen that almost all the moments of the core have finished reversing before the reversal occurs in the shell. In such situations, the interaction effect between the core and the shell helps to rotate the moments of the shell under a smaller external field. Based on this explanation, for $t = 6$ nm to $t = 8$ nm, the magnetocrystalline anisotropy field of the core plays the most significant role in determining the coercivity. It is considered that decreasing the anisotropy field of the core as t increases leads to the reduction of the coercivity.

4. Conclusions

In this work, we have systematically investigated the effects of cerium content, grain structure, and shell thickness on the coercivity of single-grain magnets. Because the addition of cerium leads to lower anisotropy, the coercivity of single $(Nd,Ce)_2Fe_{14}B$ type grain decreases as the cerium content increases. Under the same total cerium content, compared with single $(Nd,Ce)_2Fe_{14}B$ grain, core $(Ce_2Fe_{14}B)$–shell $(Nd_2Fe_{14}B)$ grain, and core $(Nd_2Fe_{14}B)$–shell $(Ce_2Fe_{14}B)$ grain, the core $((Nd,Ce)_2Fe_{14}B)$–shell $(Nd_2Fe_{14}B)$ grain with 2 nm thick shell always shows the largest coercivity. It is assumed that the grain boundary diffusion technique or the dual alloy method has potential to achieve such core $((Nd,Ce)_2Fe_{14}B)$–shell $(Nd_2Fe_{14}B)$ type grain. As for core $((Nd,Ce)_2Fe_{14}B)$–shell $(Nd_2Fe_{14}B)$ type grain with 20.51 at.% cerium, as the shell thickness t increases, the coercivity initially increases, and then quickly decreases after reaching the maximum value. With reference to such tendency of coercivity, the reasons are minutely discussed based on the positions of nucleation points. It is suggested that core $((Nd,Ce)_2Fe_{14}B)$–shell $(Nd_2Fe_{14}B)$ type grain with a proper shell thickness is beneficial to enhancing the coercivity.

References

[1] Sagawa M, Fujimura S, Togawa N, Yamamoto H and Matsuura Y 1984 *J. Appl. Phys.* **55** 2083

[2] Gutfleisch O, Willard M A, Brück E, Chen C H, Sankar S G and Liu J P 2011 *Adv. Mater.* **23** 821

[3] Hono K and Sepehri-Amin H 2012 *Scr. Mater.* **67** 530

[4] Minowa T 2008 *Resour. Geol.* **58** 414

[5] Herbst J F, Meyer M S and Pinkerton F E 2012 *J. Appl. Phys.* **111** 07A718

[6] Li Z, Liu W Q, Zha S S, Li Y Q, Wang Y Q, Zhang D T, Yue M and Zhang J X 2015 *J. Rare Earths* **33** 961

[7] Pathak A K, Khan M, Gschneidner Jr. K A, McCallum R W, Zhou L, Sun K W, Dennis K W, Zhou C, Pinkerton F E, Kramer M J and Pecharsky V K 2015 *Adv. Mater.* **27** 2663

[8] Niu E, Chen Z A, Chen G A, Zhao Y G, Zhang J, Rao X L, Hu B P and Wang Z X 2014 *J. Appl. Phys.* **115** 113912

[9] Xing M Y, Han J Z, Lin Z, Wan F M, Li C, Liu S Q, Wang C S, Yang J B and Yang Y C 2013 *J. Magn. Magn. Mater.* **331** 140

[10] Boltich E B, Oswald E, Huang M Q, Hirosawa S, Wallace W E and Burzo E 1985 *J. Appl. Phys.* **57** 4106

[11] Zhou S X, Wang Y G and Høier R 1994 *J. Appl. Phys.* **75** 6268

[12] Okada M, Sugimoto S, Ishizaka C, Tanaka T and Homma M 1985 *J. Appl. Phys.* **57** 4146

[13] Li D and Bogatin Y 1991 *J. Appl. Phys.* **69** 5515

[14] Yan C J, Guo S, Chen R J, Lee D and Yan A R 2014 *IEEE Trans. Magn.* **50** 2102605

[15] Zhu M G, Li W, Wang J D, Zheng L Y, Li Y F, Zhang K, Feng H B and Liu T 2014 *IEEE Trans. Magn.* **50** 1000104

[16] Huang S L, Feng H B, Zhu M G, Li A H, Li Y F, Sun Y C, Zhang Y and Li W 2015 *Int. J. Miner. Metall. Mater.* **22** 417

[17] Huang S L, Feng H B, Zhu M G, Li A H, Zhang Y and Li W 2014 *AIP Adv.* **4** 107127

[18] Li W, Li A H, Feng H B, Huang S L, Wang J D and Zhu M G 2015 *IEEE Trans. Magn.* **51** 2103603

[19] Zhu M G, Han R, Li W, Huang S L, Zheng D W, Song L W and Shi X N 2015 *IEEE Trans. Magn.* **51** 2104604

[20] Rong C B and Shen B G 2018 *Chin. Phys. B* **27** 117502

[21] Shang R X, Xiong J F, Liu D, Zuo S L, Zhao X, Li R, Zuo W L, Zhao T Y, Chen R J, Sun J R and Shen B G 2017 *Chin. Phys. B* **26** 057502

[22] Liu D, Zhao T Y, Li R, Zhang M, Shang R X, Xiong J F, Zhang J, Sun J R and Shen B G 2017 *AIP Adv.* **7** 056201

[23] Li R, Liu Y, Zuo S L, Zhao T Y, Hu F X, Sun J R and Shen B G 2018 *Chin. Phys. B* **27** 047501

[24] Donahue M J and Porter D G http://math.nist.gov/oommf [2018-10-10]

[25] Donahue M J and Porter D G 1999 *OOMMF User's Guide Version* 1.0 (Gaithersburg: National Institute of Standards and Technology) p. 198

[26] Sagawa M, Fujimura S, Yamamoto H, Matsuura T and Hirosawa S 1985 *J. Appl. Phys.* **57** 4094

[27] Herbst J F 1991 *Rev. Mod. Phys.* **63** 819

[28] Sang C X, Zhao G P, Xia W X, Wan X L, Morvan F J, Zhang X C, Xie L H, Zhang J, Du J, Yan A R and Liu P 2016 *Chin. Phys. B* **25** 037501

[29] Peng Y, Zhao G P, Wu S Q, Si W J and Wan X L 2014 *Acta Phys. Sin.* **63** 167505 (in Chinese)

[30] Zhang X C, Zhao G P, Xia J, Yue M, Yuan X H and Xie L H 2014 *Chin. Phys. B* **23** 097504

[31] Xia J, Zhang X C and Zhao G P 2013 *Acta Phys. Sin.* **62** 227502 (in Chinese)

[32] Zhao G P, Zhao M G, Lim H S, Feng Y P and Ong C K 2005 *Appl. Phys. Lett.* **87** 162513